

The Local Value of H_0

Adam G. Riess and Louise Breuval

Department of Physics and Astronomy, Johns Hopkins University, Baltimore, MD 21218, USA
Space Telescope Science Institute, 3700 San Martin Drive, Baltimore, MD 21218, USA

Abstract. We review the local determination of the Hubble constant, H_0 , focusing on recent measurements of a distance ladder constructed from geometry, Cepheid variables and Type Ia supernovae (SNe Ia). We explain in some detail the components of the ladder: (1) geometry from Milky Way parallaxes, masers in NGC 4258 and detached eclipsing binaries in the Large Magellanic Cloud; (2) measurements of Cepheids with the *Hubble Space Telescope* (*HST*) in these anchors and in the hosts of 42 SNe Ia; and (3) SNe Ia in the Hubble flow. Great attention to negating systematic uncertainties through the use of differential measurements is reviewed. A wide array of tests are discussed. The measurements provide a strong indication of a discrepancy between the local measure of H_0 and its value predicted by Λ CDM theory, calibrated by the cosmic microwave background (*Planck*), a decade-long challenge known as the ‘Hubble Tension’. We present new measurements with the *James Webb Space Telescope* of >320 Cepheids on both rungs of the distance ladder, in a SN Ia host and the geometric calibrator NGC 4258, showing reduced noise and good agreement with the same as measured with *HST*. This provides strong evidence that systematic errors in *HST* Cepheid photometry do not play a significant role in the present Hubble Tension. Future measurements are expected to refine the local determination of the Hubble constant.

Keywords. Hubble constant, Cepheids, supernovae, parallaxes

1. Why care about the Hubble Constant?

The Hubble constant, H_0 , is a measure of the present expansion rate of the Universe and may be used to infer related quantities such as the age of the Universe, its fate, the distance to galaxies (with known redshifts), etc. Connecting the measured value of the Hubble constant to related properties of the Universe tests our fundamental understanding of our cosmic paradigm.

In the local Universe, $z \sim 0$, H_0 is given by the constant of proportionality between distances, D , and redshifts, z , in the relation $cz = H_0 D$. More generally, i.e., at $z > 0$ and $t < t_0$ (where t_0 refers to the present era) the relation between distance and redshift may evolve and so is more generally defined as

$$D = \frac{cz}{H_0} \left\{ 1 - \left[1 + \frac{q_0}{2} \right] z + \left[1 + q_0 + \frac{q_0^2}{2} - \frac{j_0}{6} \right] z^2 + O(z^3) \right\},$$

which follows from a Taylor expansion of the increasing scale factor, a :

$$a(t) = a_0 \left\{ 1 + H_0 (t - t_0) - \frac{1}{2} q_0 H_0^2 (t - t_0)^2 + \frac{1}{3!} j_0 H_0^3 (t - t_0)^3 + O([t - t_0]^4) \right\},$$

with $H(t) = +(da/dt)/a$ the expansion rate at time t , $q(t) = -(d^2a/dt^2) [H(t)]^{-2} / a$ the deceleration parameter, and $j(t) = (d^3a/dt^3) [H(t)]^{-3} / a$ the jerk parameter, and so on. As provided, these relations ignore curvature but terms for a non-flat Universe can be included. Thus seen, the Hubble ‘constant’ is the present value of the expansion $H_0 = H(t_0)$ today. The higher-order derivatives of expansion, q_0 and j_0 , can be directly determined from this relation, provided a set of distance and redshifts measurements covering a wide range of redshift is available (e.g., with Type Ia supernovae, SNe Ia, at $0 < z < 1$ free of cosmological model

assumptions). This approach, following the definition, is called the ‘Direct’ route, because it does not invoke a cosmological model and has negligible dependence on gravity.

The alternative route to knowledge of H_0 comes from predicting its present value from fine calibration of the cosmological model, (‘Vanilla’) Λ cold dark matter (Λ CDM), measured from the cosmic microwave background (CMB). By invoking Λ CDM we are referring to a description of the Universe as composed of the simplest dark matter (i.e., non-interacting, non-decaying, from a particle with only gravitational interactions), the simplest dark energy (i.e., a ‘Cosmological Constant’), atoms, photons, and neutrinos (three species), without spatial curvature, and *without any other cosmologically important features* (hence ‘Vanilla’). We can use the model as it would have looked at $z > 1000$ to predict the physical size of fluctuations in the primordial plasma and compare the fluctuation spectrum with their angular size as observed from the CMB. This comparison serves to calibrate the six free parameters in Λ CDM. Once calibrated, the model predicts that dramatic changes in the Universe will occur (matter dominated followed by vacuum energy dominated) and describes the expansion history, $H(z)$, from $z = 1000$ to $z = 0$, and hence the value of H_0 . In the appendix we provide a detailed description of how, in practice, the value of H_0 is measured from the CMB. We encourage the reader to review it, as it may challenge the prior belief that this is simple! See [Kamionkowski and Riess \(2022\)](#) and [Planck Collaboration et al. \(2020\)](#) for details. As should be clear, Λ CDM is a *phenomenological* model with parameters that stand in for a physical description of the unknown nature of 96% of the present Universe. Thus, H_0 is uniquely suited to provide an ‘end-to-end’ test of Λ CDM and our understanding of the Universe. By comparing the direct and model-dependent routes, we can test the model. Figure 1 illustrates this test.

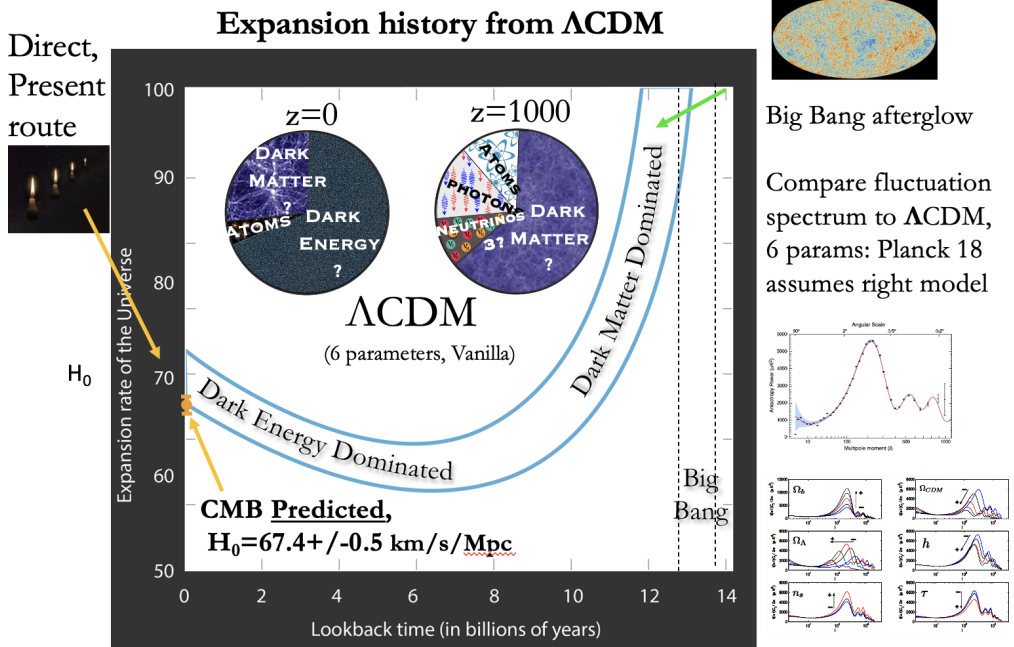


Figure 1. The expansion rate of the Universe can be predicted by the Λ CDM model with its parameters calibrated by the CMB or measured directly and locally from redshifts and distances.

2. The Distance Ladder: From Geometry to Cepheids to Type Ia Supernovae

Because the indirect route offers better than percent-level precision, fully leveraging the comparison demands a percent-level local measurement. The first generation of such measurements from the *Hubble Space Telescope* (*HST*) Key Project (KP; see [Freedman and Madore 2023](#), in this conference), foundational work of immense importance, reached 10% precision by 2001 (see also [Sandage et al. 2006](#)). To reach greater precision requires a considerable redesign of the approach and methods to reach percent-level while at the same time leveraging new geometric measurements (e.g., the ESA *Gaia* mission parallaxes). In 2005 we started the SHOES program to use new instruments on the *HST* to accomplish this. The SHOES ladder is composed of three components or "rungs": Geometry to Cepheids to Type Ia supernovae. The critical, new elements of SHOES are:

- Cancel flux calibration errors using *HST* to measure all Cepheids (rung 1 and 2);
- Observe all Cepheids in the Near-Infrared (NIR) to minimize dust;
- Use best quality SN data, consistently calibrated (Pantheon+, [Brout et al. 2022](#));
- Comprehensive error analysis, include covariance, analyze plausible variants;
- Publicly release data, 10^7 data numbers, and code to fit the data.

2.1. Geometric Rung

There are three geometric anchors of the distance ladder which rely on different systems and measurements and so are fully independent of each other. Milky Way Cepheid parallaxes, thanks to *Gaia* (now in Data Release 3) provide $\sim 1\%$ precision in the calibration of the Hubble constant. These are a tremendous advancement over past work. However, we could not leverage the geometric precision these afford without an equally precise photometric tie. The SHOES project has spent a lot of effort to developing a spatial scanning method for photometric measurements of ultra bright targets with *HST* that demonstrates extreme precision and accuracy for direct calibration of Cepheids on the second rung (in SN Ia hosts). These scans were also previously used to measure parallaxes (before *Gaia*). More recently, even greater precision and independence from *Gaia* systematics (the parallax offset term) has come from Cepheids in open star clusters, where hundreds of stellar parallaxes may be averaged ([Riess et al. 2022a](#)). Figure 2 shows three different approaches to measuring Cepheid parallaxes, all in good agreement.

Another anchor comes from the exquisite detached-eclipsing binary measurements in the Large Magellanic Cloud (LMC; [Pietrzyński et al. 2019](#)) which reach 1.2% precision. Again, leveraging these requires direct measurements of Cepheids with *HST*. These measurements ([Riess et al. 2019](#)) yield both greater precision and accuracy, especially in the NIR, than those from the ground (see past ground data in [Freedman and Madore 2023](#), in this conference) with a dispersion of ~ 0.07 mag. They also demonstrate the power of NIR data to mitigate dust and the use of colors to deredden for remaining dust. These are shown in Figure 3.

The third anchor is the water-maser host NGC 4258, with a 1.5% geometric distance ([Reid et al. 2019](#)). By collecting Cepheids in six fields, the SHOES Team has collected 669 Cepheids in NGC 4258 ([Yuan et al. 2022](#)). The Cepheids in NGC 4258 also provide a strong test of the effect of the blotchy background on Cepheid photometry, because we can compare the Cepheid intercepts measured in the inner region (where crowding is high) versus in the outer region, where it is low. As shown in Figure 4, the agreement is good, at the ~ 0.05 mag level. Here we clarify some terminology. [Freedman and Madore \(2023\)](#), at this conference, referred to crowding as a bias in photometry. To be clear, this term (as shown in that contribution) is the measured difference in the background level between the true sky and the mean level of the (non-Cepheid) stars (measured with artificial stars). Thus, the true (Cepheid) background is both components added together. Accounting for these results in *no bias*, but due to the variations in the latter, it does lead to greater statistical noise which is not 'unexplained' but,

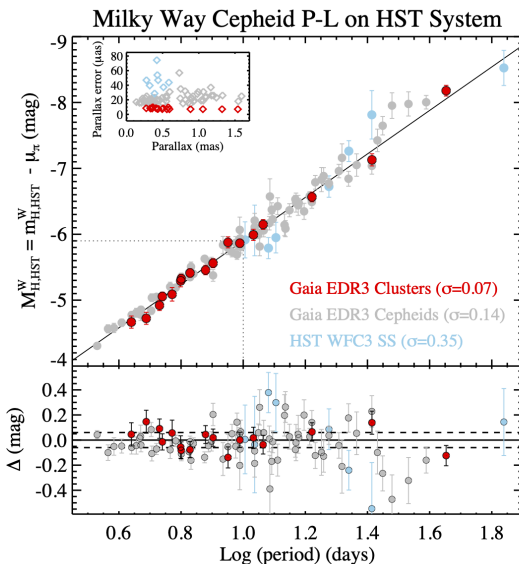


Figure 2. The Milky Way Cepheid period–luminosity relation in the *HST* NIR, reddening-free (Wesenheit) system as calibrated with three samples. Parallaxes from *HST* spatial scanning (Riess et al. 2018) for 8 Cepheids are in blue and yield 3% precision. The 68 points in gray (Riess et al. 2021) using *Gaia* early Data Release 3 (EDR3) parallaxes with simultaneous calibration of the parallax offset. The red points come from cluster Cepheids and do not require parallax offset calibration as they are measured in the range where *Gaia* is best calibrated (Riess et al. 2022a). These samples differ in their parallax precision (inset) leading to the low dispersion of $\sigma = 0.07$ mag for the cluster Cepheids.

rather, measured from the artificial stars and included in the measurement errors. Multiple tests such as the one above show that the photometry is accurate and provided that one has access to more than ~ 25 Cepheids per host, the noise does not reach the level of the uncertainty in the SNe Ia the Cepheids calibrate.

2.2. SNe Ia calibrations

The next rung in the distance ladder is the consistent measurement of Cepheid variables in the hosts of recent SNe Ia. Cepheids can be measured effectively with *HST* up to $z \sim 0.01$ or $D < 40$ Mpc, a volume that produces a prototypical SN Ia with low reddening about once a year. Because each SN Ia yields a distance with $\sim 6\%$ precision, we need to collect many dozens in order to reach the target goal. The SH0ES team has now collected 42 SNe Ia in 37 hosts, an effort requiring about 1000 orbits of *HST*, resulting from more than a dozen Time Allocation Committee-selected proposals. These SNe necessarily come from the last four decades, the era of digital measurements and from many SNe surveys. The SNe measurements are standardized across many surveys by the Pantheon+ collaboration using all-sky surveys.

The Cepheids are found in these hosts primarily with a white light filter and then followed up in the optical (V and I bands) and the NIR (H band). It is important to note that the optical measurements are not ‘random-phase’ as claimed in the previous contribution (see Freedman and Madore 2023, in this issue); they are at known phases due determined from the simultaneous white-light light curves and, thus, are used to measure the magnitudes at mean phase. Composite light curves of all Cepheids in all hosts are shown in Figure 5. These are used to identify Cepheids and determine their periods. The individual period–luminosity relations are

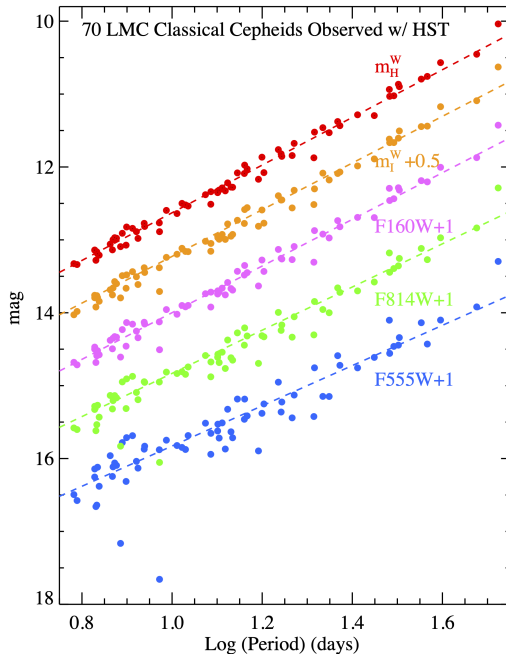


Figure 3. Period-mean magnitude relation for the 70 LMC Cepheids observed with *HST* using DASH mode.

shown in Figure 6. The number of Cepheids varies but has a mean of around 50 Cepheids per host.

Because this conference is focused on Cepheid variables, we can take a closer look at the extragalactic Cepheids and address the question if they are like those in the Milky Way. Naturally we would think so, but we can also bin their light curves by period and compare the changing shape to the well-known Hertzsprung progression. There is a rather striking match, as shown in Figure 7. The light curves at short periods are symmetric and as the periods grow, become more asymmetric and with higher amplitudes before becoming more shallow and sinusoidal-looking at long periods. There are also fine features like the bump which evolves with period to be earlier in phase due to a resonance between an overtone and fundamental oscillation.

The final rung is the measurement of the Hubble flow from SNe Ia at moderate redshifts. We made these measurements from ~ 300 SNe Ia from the Pantheon+ sample at $0.023 < z < 0.15$. This redshift range was chosen to avoid the largest, local peculiar motions while avoiding the highest redshifts to avoid sensitivity to higher-order terms, q_0 and j_0 . We correct for peculiar velocities using mass maps and determine $q_0 = -0.55$ ($j_0 = 1$) from high-redshift SNe Ia. The global fit of the distance ladder and H_0 is a large set of simultaneous, linear equations which can be optimized for five global parameters, including the fiducial luminosity of SNe Ia and Cepheids, two parameters specific to Cepheids, the slope of their period–luminosity relation and metallicity dependence, and the final parameter is ($5 \log H_0$). The entire data set as fitted is shown in Figure 8. The equations can be solved exactly by inverting a matrix, but we also use a brute-force, Markov Chain Monte Carlo approach to view the interdependency of parameters.

One of the more interesting parameters for this group is the Cepheid metallicity dependence. We find a value of $-0.22 \pm 0.04 \text{ mag dex}^{-1}$, which sits well in the middle range of recent findings. Figure 9 shows a summary of metallicity results: we see that the metallicity

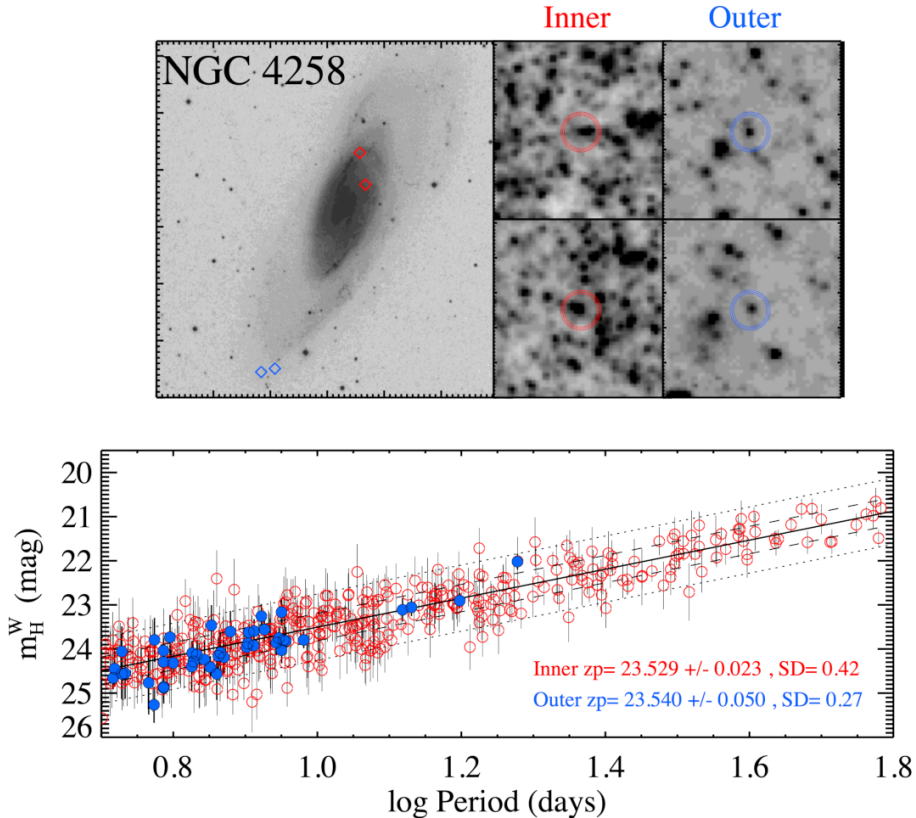


Figure 4. Comparison of Cepheids measured in a dense (inner) field (in red) and sparse (outer) field (in blue) of NGC 4258. Because these Cepheids are at the same distance, the comparison shows the accuracy of the background estimates, which differ in the mean over the same sampled range, $0.7 < \log P < 1.2$ [days], by 0.45 mag (relative to the Cepheids) yet yield a consistent intercept with $\sigma = 0.05$ mag. The difference in metallicity between the samples, ~ 0.08 dex, corresponds to a difference of 0.02 mag, smaller than the precision of this comparison.

effect (γ) has now converged to a modest range of values with wide concurrence on a negative sign, with a good agreement between various measurements from independent teams and methods. Although a few studies diverge from this central value, [Breuval et al. \(2022\)](#) identified that these measures were affected by geometry effects in the Magellanic Clouds and by the use of an atypical *Gaia* parallax zero-point in the Milky Way. Overall we find strong evidence, from dozens of calibrations in the literature, that metal-rich Cepheids are brighter than metal-poor ones by ~ 0.2 mag dex $^{-1}$. There is also agreement on the size and sign between the empirical measurements and theoretical modeling (presented at this meeting) of Wesenheit magnitudes (the only disagreement with the theory was on the monochromatic dependence) with Wesenheit magnitudes of greatest relevance for distance measurements. However, it is important to note that the value of the Hubble constant is not sensitive to this parameter, because the mean metallicity of the SNe Ia hosts is similar to the mean of the anchors. The anchors themselves have somewhat different metallicities, so the metallicity term is an important contributor to the consistency of the anchors.

The resulting determination of H_0 is 73.04 ± 1.04 km s $^{-1}$ Mpc $^{-1}$, in good agreement with the mean of local determinations but inconsistent with the prediction of 67.4 ± 0.5 km s $^{-1}$ Mpc $^{-1}$ at the 5σ confidence level. This discrepancy is so famous, it has a name, the

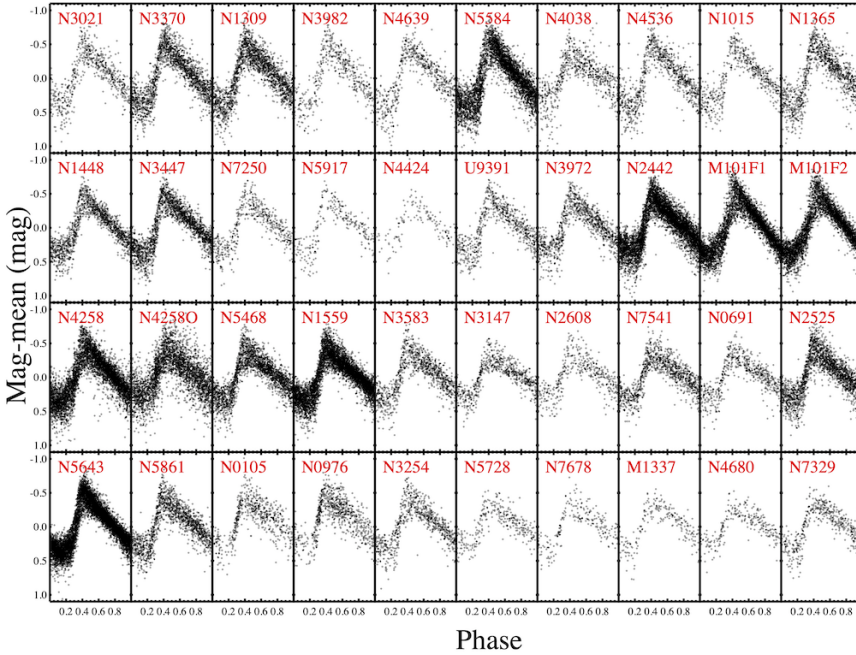


Figure 5. Composite visual (F555W) or white-light (F350LP) Cepheid light curves. Each *HST* Cepheid light curve with $10 < P < 80$ days is plotted after subtracting the mean magnitude and determining the phase of the observation.

‘Hubble Tension’, and it has been disturbing the cosmology community for a decade. It is certainly tempting to think the discrepancy may be telling us we are missing something in the cosmological model.

We also calculated 67 variants of the analysis varying many, many, many things. There are too many to discuss them all, but we select a subset of the most interesting and what value of H_0 they yield.

Variants

- Optical Cepheid data only (72.7)
- Different peculiar velocity map or none (73.1, 72.7)
- SN scatter monochromatic + mass step (73.5)
- No pre-2000 SNe (73.2)
- Closest half hosts (73.1)
- Most crowded half (73.4)
- Least crowded half (73.3)
- Skip ‘local hole’ $z > 0.06$ (73.4)
- All host types (73.3)
- Include tip of the red-giant branch (consistent) jointly (72.5)
- No metallicity term (73.5)
- Break in the period–luminosity relation at $P = 10$ days (72.7)
- No extinction correction (74.8)
- Individual host extinction law (73.9)
- Free parametric extinction law (73.3)
- Low $R_V = 2.5$ extinction law (73.2)

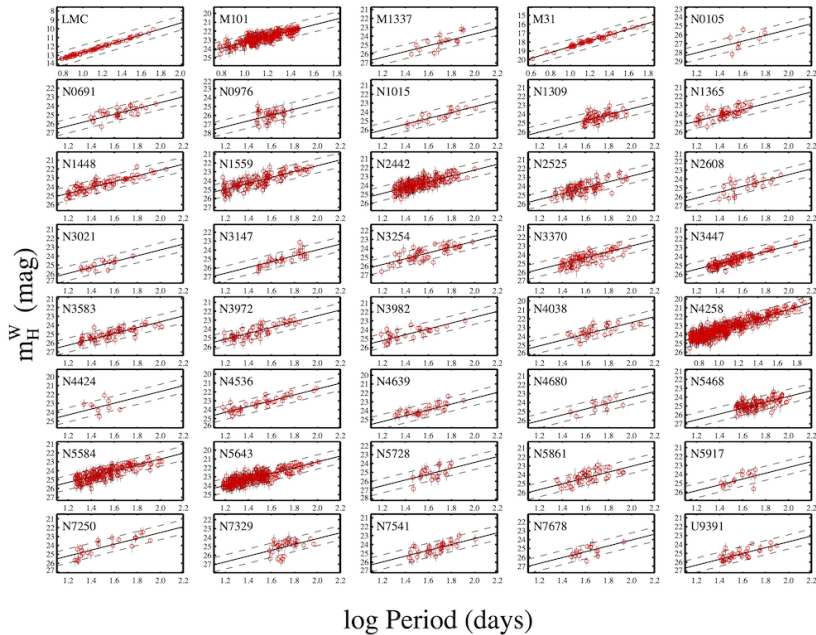


Figure 6. *HST* NIR Cepheid period–Wesenheit index relations. The Cepheid magnitudes are shown for 37 SNe Ia hosts, M31, and two of the three possible distance-scale anchors (LMC and NGC 4258). The uniformity of the photometry and metallicity reduces systematic errors along the distance ladder. A single slope is shown and used for the baseline, but we also allow for a break (two slopes) as well as limited period ranges in some analysis variants.

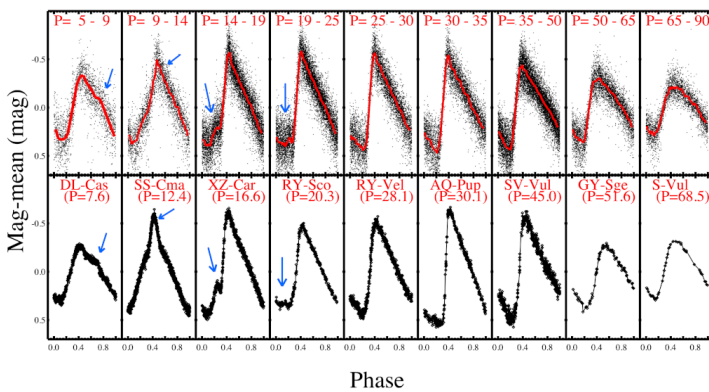


Figure 7. Composite visual (F555W) or white-light (F350LP) Cepheid light curves binned by period (top) and compared with individual Milky Way Cepheids near the middle period of the bin. The ‘Hertzsprung progression’ (the relation between the light-curve shape and the period) is apparent, including subtle features like the progression in phase of a resonance ‘bump’ between the second overtone and fundamental pulsation for $P < 20$ days. The red line is a cubic spline constrained by the averages of bins in phase.

- Two of three anchors (73.0, 73.4, 73.2)
- No outlier rejection (73.4)

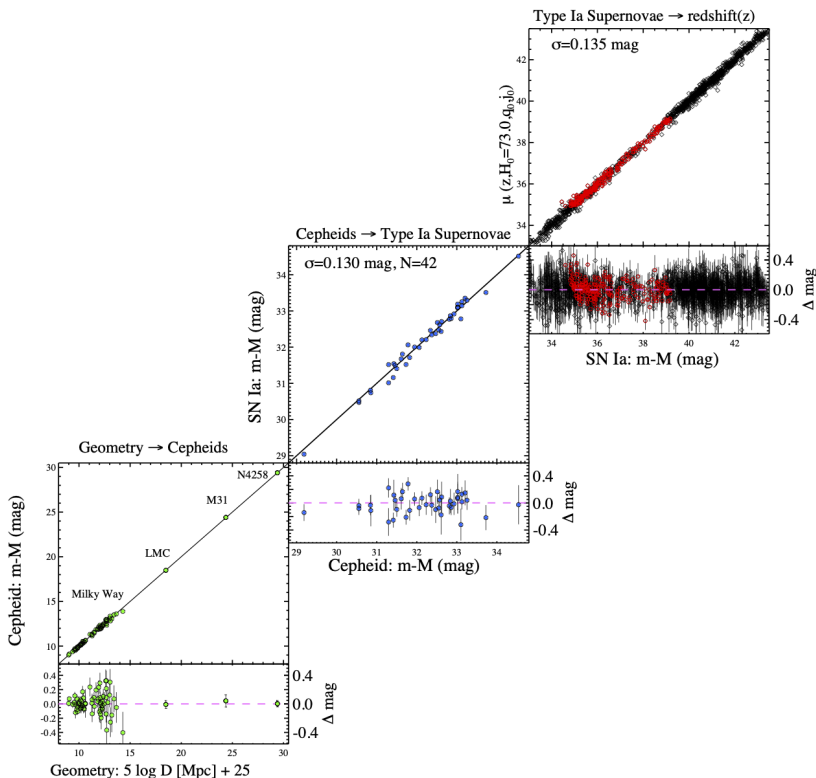


Figure 8. Complete distance ladder (Riess et al. 2022b). The simultaneous agreement of distance pairs: geometric and Cepheid-based (bottom left), Cepheid- and SN-based (middle), and SN- and redshift-based (top right) provides the measurement of H_0 . For each step, geometric or calibrated distances on the abscissa serve to calibrate a relative distance indicator on the ordinate through the determination of M_B or H_0 . Results shown are an approximation to the global fit, as discussed in the text. Red SN points are at $0.0233 < z < 0.15$, with the lower-redshift bound producing the appearance of asymmetric residuals when plotted against distance.

As shown, it is hard to move the value of the Hubble constant much below 72.5 or much above 73.5, which indicates that the baseline result is fairly robust. Although the SH0ES team measurement provides the highest precision, a consequence of having the largest sample of calibrated SNe Ia, the Hubble Tension is a broad finding that has lasted a decade and covers a wide range of different techniques, teams and methods. A recent summary of many measures is shown in Figure 10. This is a subset of recent measures but selected to be those which are the most cited, offer the most independence, and use the best source of data when multiple are available (e.g., *HST* versus ground).

3. What can we learn from *JWST*?

There are many tests of the distance ladder to discuss, but in the interest of space, we will focus on the most recent and novel from the *James Webb Space Telescope (JWST)*. Observations with the *JWST* offer for the first time the resolution in the NIR (and mid-IR) to separate Cepheids from their stellar crowds. This greatly reduces the noise in the period–luminosity relations, whose source was the variations in background (i.e., primarily fluctuations in the density of red giants) seen at *HST* NIR resolution. The previous contribution (see Freedman and Madore 2023, this volume) presented their group’s *JWST* observations

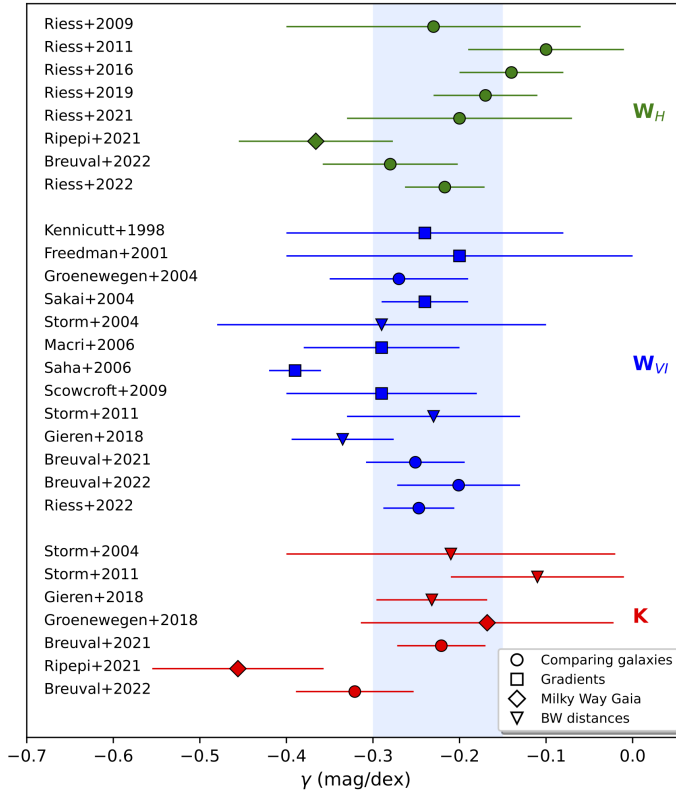


Figure 9. Recent Cepheid metallicity measurements. There is good consistency on the sign (negative) and scale, -0.1 to $-0.3 \text{ mag dex}^{-1}$, for this term. It is important to know that this term has little effect on H_0 because the mean metallicity of Cepheids on the first and second rung is similar.

following up Cepheids discovered with *HST* in the SN Ia host NGC 7250. They showed 14 Cepheids with a dispersion of 0.22 mag at $1.15 \mu\text{m}$, half the size of the dispersion seen with *HST* in the NIR (see also the wonderful contribution by Kayla Owens presenting this work). This is consistent with what we see in our *JWST* observations.

We observed >320 Cepheids in two hosts, NGC 5584 (the host of a SN Ia) and NGC 4258, the previously discussed calibrator. We observed the Cepheids in three filters centered at 0.9 , 1.5 and $2.8 \mu\text{m}$ and across two epochs separated by 2–3 weeks. The differences in epochs allowed us to (1) confirm the astrometric identification of the Cepheids through their variability; (2) check the photometric stability of *JWST* over time by comparing non-variable stars; and (3) constrain the phase of the Cepheids (knowledge of which has dissipated over the years since they were discovered).

In Figure 11 we show the use of the epoch differences applied to the Cepheid phases. We found that the combination of two epochs (to reduce the random phase error) and the ability to constrain the phase reduced the dispersion from $\sim 0.43 \text{ mag}$ to $\sim 0.17 \text{ mag}$, which is equivalent in statistical leverage to doubling the sample size. The results for both hosts and direct comparison with *HST* is shown in Figure 12. In Figure 13 we show a comparison of many postage stamps around Cepheids with *HST* and *JWST*. The contrast offered by *HST* is excellent in the optical, but becomes low, and the crowding high, in the NIR. This is the region where *JWST* wins by a large margin. The filters F160W for *HST* and F150W for *JWST* are nearly the same, which offers the best comparison.

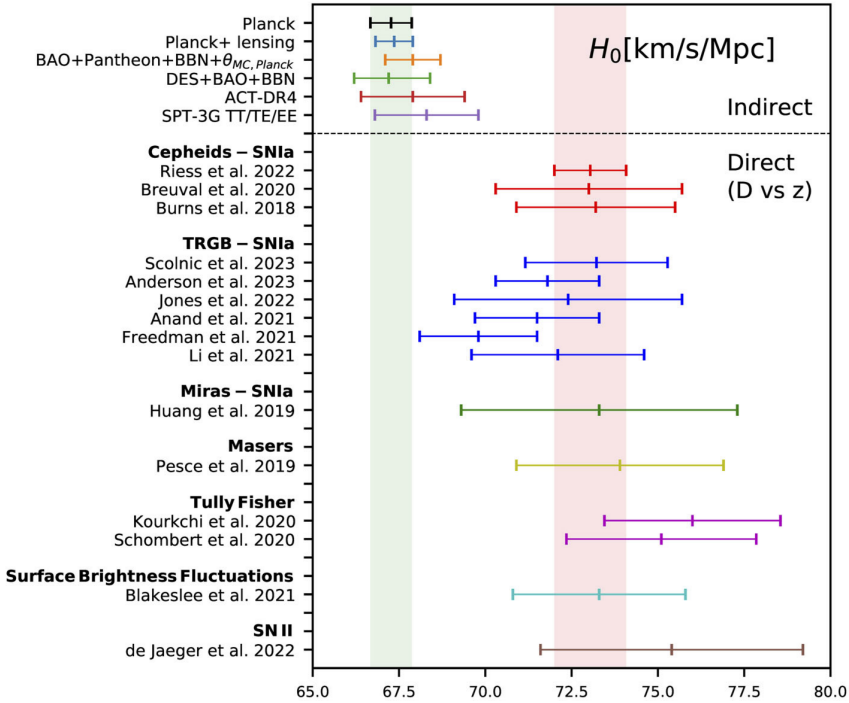


Figure 10. Recent measures and the Hubble Tension. The subset of recent measures was selected to be those which are the most cited, offer the most independence, and use the best source of data when multiple are available (e.g., *HST* versus ground).

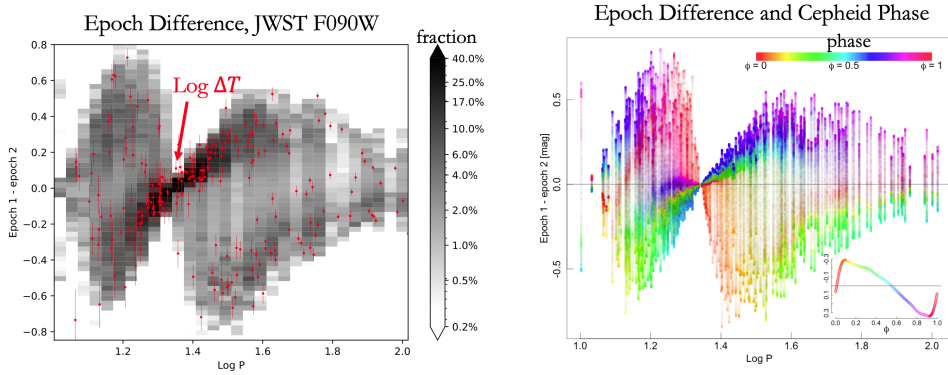


Figure 11. *JWST* two-epoch measurements of Cepheids in NGC 5584. (left) Epoch differences. (right) The expected differences which determine the phase.

Because we have measured Cepheids with *JWST* at both rungs, an SN Ia host and NGC 4258, we can directly measure and compare the resulting calibration they provide for the distance ladder, a difference which is independent of uncertainties in the zero points of *JWST*, which cancel out. As shown in the inset of Figure 12, they provide a consistent difference (in magnitudes) between rungs as seen with *HST*. Because the Cepheid samples are large (>320

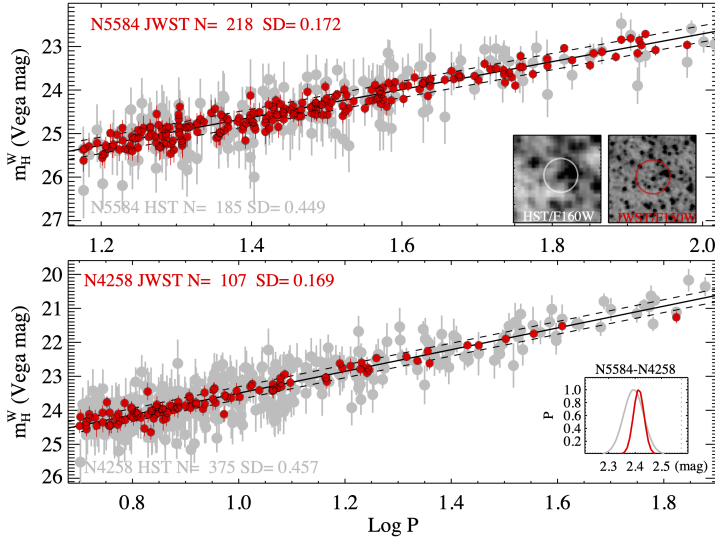


Figure 12. Comparison with the standard (SH0ES; Riess et al. 2022b) magnitude $W_{V,I}^H$ period–Wesenheit relation used to measure distances. The red points use JWST F150W, and the gray points are from HST F160W, including a small transformation, $F150W - F160W = 0.033 + 0.036[(V - I) - 1.0]$. The top panel is for NGC 5584, with the inset showing image stamps of the same Cepheid seen in the H band by each telescope. The bottom panel is for NGC 4258, with the inset showing the difference in distance moduli between NGC 5584 and NGC 4258 as measured with each telescope.

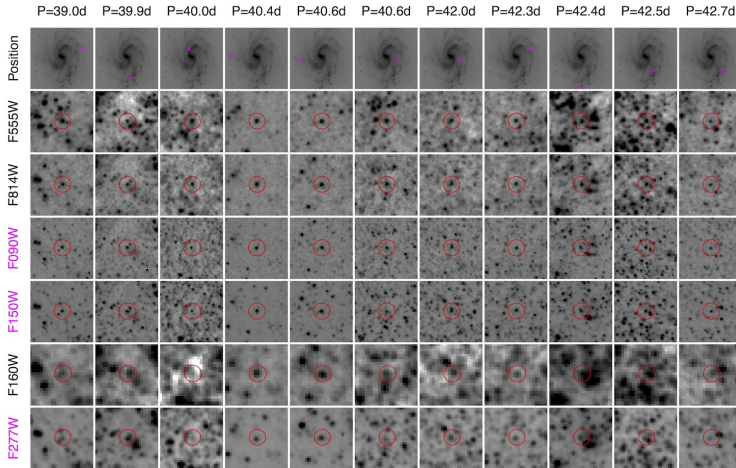


Figure 13. HST and JWST image stamps of NGC 4258 for all Cepheids with periods of 18–41 days. The top row indicates the location of each Cepheid. HST filters are labeled in black and JWST filters in magenta.

with JWST compared with >560 with HST) and this is purely a test of Cepheid measurements, the precision of this test is very high, 0.04 mag, many times smaller than the 0.18 mag size of the Hubble Tension. So, by stripping the noise and crowding from the Cepheid measurements with HST, these observations provide the strongest evidence yet that systematic errors in HST Cepheid photometry do not play a significant role in the present Hubble Tension (Riess et al.

2023). However, a more ambitious goal which will require more observations and the work of many is to improve the precision of the local measurement of H_0 to reach 1.0%.

So, what causes the Hubble Tension? We do not know. The facts are that it has lasted 10 years, it is statistically very significant and all precise (e.g., $\leq 3\%$) local ladder measurements are higher than the CMB-based prediction, so it is pretty robust. We have undertaken a rather exhaustive set of tests and studies of systematics and there has been no indication of a problem on the measurement side. In this regard the *JWST* data are very impressive. One can speculate about an unknown systematic error, but the data have become very good, so concrete proposals for such systematics are inconsistent to date with the breadth of data and tests. It is also easy to speculate that it is something missing in Λ CDM but much harder to come up with a specific notion of what that is with sufficient rigor to test and yield a better fit to the cosmological data. This is a very hot topic in the theory community and we are seeing lots and lots of proposals, but nothing definitive or compelling (yet). We are optimistic. History has shown that basic errors are found by our community rapidly (timescale of \sim months) and that discrepancies that last this long are usually telling us something interesting and thus worth the investment. Let's be curious.

(On another day the conference enacted a poll, which is a rather unscientific way to resolve the Hubble Tension but it is a snapshot of what people at the conference thought after a couple of days, and entertaining, and we attach the result as Figure 14. The polling was anonymous and used a smartphone app to allow the participants to vote. The three options voted on as possible cause of the Hubble Tension were a problem with the CMB analysis, a problem with Λ CDM or an issue with stellar physics. As the conference was a gathering of people studying stars and their physics, it was noteworthy that $\sim 70\%$ of attendees did not think the Hubble Tension was due to a problem with the physics of stars).

We want to thank the organizers for a wonderful conference filled with discussions and goulash.

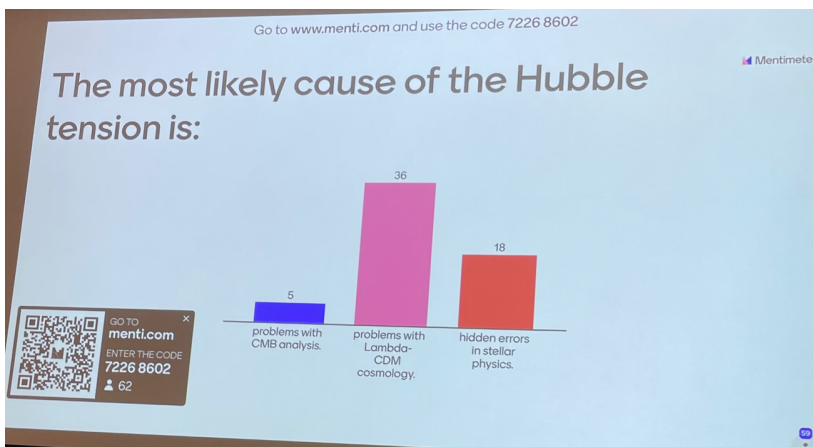


Figure 14. Meeting Poll.

References

- Breuval, L., Riess, A. G., Kervella, P. et al., 2022, ApJ 939, 89
 Brout, D., Taylor, G., Scolnic, D., et al., 2022, ApJ 938, 111
 Freedman, W. L. & Madore B. F., 2023, arXiv:2308.02474

- Kamionkowski, M. & Riess, A. G., 2022, arXiv:2211.04492
 Pietrzyński, G., Graczyk, D., Gellenne, A., et al., 2019, *Nature* 567, 200
 Planck Collaboration, Aghanim, N., et al., 2020, *A&A* 641, A6
 Reid, M. J., Pesce, D. W. and Riess, A. G., 2019, *ApJL* 886, L27
 Riess, A. G., Casertano, S., Yuan, W., et al., 2021, *ApJ* 855, 136
 Riess, A. G., Casertano, S., Yuan, W., et al., 2019, *ApJ* 876, 85
 Riess, A. G., Casertano, S., Yuan, W., et al., 2021, *ApJL* 908, L8
 Riess, A. G., Breuval, L., Yuan, W., et al., 2022, *ApJ* 938, 36
 Riess, A. G., Yuan, W., Macri, L. M., et al., 2022, *ApJL* 934, L7
 Riess, A. G., Anand, G. S., Yuan, W., et al., 2023, arXiv:2307.15806
 Sandage, A., Tammann, G. A., Saha, A., et al., 2006, *ApJ* 653, 843
 Yuan, W., Macri, L. M., Riess, A. G. et al., 2022, *ApJ* 940, 64

Appendix A. From the CMB to H_0 , a primer

The first and strongest peak we see in the power spectrum (expansion into spherical harmonics), l_s , determines the angle subtended by the sound horizon, the distance a fluctuation in the plasma will travel at the sound speed from the time of the Big Bang to the surface of last scattering (i.e., $z \sim 1000$). This scale results from the angular size of this feature, $\ell_s \simeq 2/\theta_s$. The angle subtended by the sound horizon is $\theta_s = r_s/D_A$, where D_A is the angular-diameter distance to the CMB surface of last scatter, and $r_s \sim c_s t_{\text{dec}}$ is the sound horizon. The angle is exceedingly well-measured by *Planck*: $\theta_s = (1.04109 \pm 0.00030) \times 10^{-2}$ rad.

We can calculate the physical size of the sound horizon from the physics of the early Universe as given by Λ CDM. It follows by integrating the sound speed $c_s(t)$ over time prior to recombination and is given by the integral,

$$r_s = \int_{z_{\text{ls}}}^{\infty} \frac{c_s(z) dz}{H(z)} = \frac{c}{\sqrt{3}H_{\text{ls}}} \int_{z_{\text{ls}}}^{\infty} \frac{dz}{[\rho(z)/\rho(z_{\text{ls}})]^{1/2} (1+R)^{1/2}}, \quad (1)$$

over redshift z . Here, $z_{\text{ls}} \simeq 1080$ is the redshift at which CMB photons last scatter, $c_s(z) = c [3(1+R)]^{-1/2}$ is the sound speed of the photon–baryon fluid, with $R = (3/4)(\omega_b/\omega_\gamma)/(1+z)$, and $\rho(z)$ is the total energy density at redshift z . Here, $\omega_b = \Omega_b h^2$ is the current physical baryon density, where $h \equiv H_0/(100 \text{ km s}^{-1} \text{ Mpc}^{-1})$ is a dimensionless Hubble constant. ω_b is a parameter constrained by higher-peak features in the CMB power spectrum (Silk damping at higher l and the relative heights of the even- and odd-numbered peaks with ω_m) and $\omega_\gamma = 2.47 \times 10^{-5}$ is the physical photon energy density given by COBE FIRAS. It is convenient to define the expansion rate at last scattering,

$$H_{\text{ls}} = 100 \text{ km s}^{-1} \text{ Mpc}^{-1} \omega_r^{1/2} (1+z_{\text{ls}})^2 \sqrt{1 + \frac{\omega_m}{\omega_r} \frac{1}{1+z_{\text{ls}}}}, \quad (2)$$

where $\omega_m = \Omega_m h^2$ is the present physical matter density fit from the higher-peak structure in the CMB. In the standard cosmological model, the early-Universe energy density is $\rho(z) \propto \omega_m(1+z)^3 + \omega_r(1+z)^4$. The physical radiation density is

$$\omega_r = \left[1 + \frac{7}{8} N_{\text{eff}} \left(\frac{4}{11} \right)^{4/3} \right] \omega_\gamma, \quad (3)$$

where the second term accounts for additional non-relativistic degrees of freedom. In the standard cosmological model, these include the three neutrino mass eigenstates, and $N_{\text{eff}} = 3.06$.

The (comoving) angular-diameter distance to the surface of last scattering is then an integral,

$$D_A = \frac{c}{H_0} \int_0^{z_{\text{ls}}} \frac{dz}{[\rho(z)/\rho_0]^{1/2}}, \quad (4)$$

from recombination until the current time t_0 , when the total energy density is ρ_0 . The denominator here is $\rho(z)/\rho_0 = \Omega_m(1+z)^3 + (1-\Omega_m)(1+z)^{-3(1+w)}$ in the standard cosmological model, with a dark-energy equation-of-state parameter w . The cosmological constant corresponds to $w = -1$.

From $\theta_s = r_s/D_A$, we infer a Hubble constant,

$$H_0 = \sqrt{3}H_{\text{ls}}\theta_s \frac{\int_0^{z_{\text{ls}}} dz [\rho(z)/\rho_0]^{-1/2}}{\int_{z_{\text{ls}}}^{\infty} dz [\rho(z)/\rho(z_{\text{ls}})]^{-1/2} (1+R)^{-1/2}} \quad (5)$$

from the CMB.

By this route, H_0 depends on ω_b , ω_m , ω_γ , N_{eff} and also (to a lesser degree) on the other model parameters through degeneracies in the description of the fluctuation spectrum.